Thermodynamics of a Carbon Nano-Materials Based Icing Protection System for Unmanned Aerial Vehicle

Kim Lynge Sørensen
Autonomous Marine Operations and Systems Research Centre
Norwegian University of Science and Technology
O. S. Bragstads Plass 2D
NO-7491, Trondheim, Norway
kim.sorensen@itk.ntnu.no

Tor Arne Johansen
Autonomous Marine Operations and Systems Research Centre
Norwegian University of Science and Technology
O. S. Bragstads Plass 2D
NO-7491, Trondheim, Norway
tor.arne.johansen@itk.ntnu.no

Abstract—**Changes to the aerodynamic surfaces due to ice accretion are common causes for unmanned aerial vehicle (UAV) incidents in regions where the environmental conditions sustain icing conditions. For fixed wing UAVs the leading edge of airfoil surfaces is one of the primary surfaces exposed to these changes, causing a significant reduction in aerodynamic ability, i.e. decreasing lift and manoeuvrability, and increasing drag, weight, and consequently power consumption. Mitigating or altogether preventing ice accretion could potentially prevent icing related UAV incidents and increase the operability of UAVs. In recent years, proposed mitigating solutions to ice accretion (ice protection systems - IPS) make use of an electrically powered thermal source applied to the leading edge of airfoils. Such solutions are naturally highly susceptible to energy dissipation, i.e. energy lost to the surroundings and airfoil, due to thermal flux. This paper investigates the thermodynamic system, consisting of the aircraft aifoil, a thermal source, and ambient conditions, as energy is supplied to the thermal source, by an external energy supply. The thermal source, referred to in the work presented here, is an electrically conductive coating (or paint) - based on carbon nano-materials - which is part of an IPS that has been proposed for small UAVs. The investigation is based on numerical simulations applying a transient finite element approach to account for the multidimensional boundary conditions that vary along the chord of the airfoil.**

TABLE OF CONTENTS

1. INTRODUCTION

The last decade has seen the use of unmanned aerial vehicles (UAVs) increase dramatically. The primary field of application has been within the intelligence, surveillance and reconnaissance industries, but due to the applicability of UAVs, research into solutions for alternative purposes is rapidly growing, e.g. maritime search and rescue operations [1]. Part of the reason for this surge in UAV research and development is that they are a low-cost and safe alternative to manned flights, something that is increasingly relevant, especially regarding operations conducted in harsher environments, such as (but not exclusively) maritime and the Arctic.

Conducting UAV operations in environments (or regions) that sustain potential icing conditions, i.e. any region experiencing freezing temperatures and moderate to high levels of humidity, with the Arctic or Antarctic representing high-risk regions [2], [3], ice accretion on aerodynamic surfaces are common causes for UAV incidents. The leading edge of airfoils is one of the primary aerodynamic surfaces exposed to icing, which significantly reduces the airfoils aerodynamic ability, i.e. decreasing lift and manoeuvrability, while increasing drag, weight, and consequently power consumption [4].

Icing on the leading edge of an aircraft airfoil can be mitigated by an ice protection system (IPS). For manned flights, such a system is usually manually activated. Most IP Systems fall into one of two categories: thermal, or pneumatic based systems. Thermal based systems are designed to either melt the ice as it forms on the airfoil (a de-icing approach), or ensure that ice cannot form (an anti-icing approach), by the use of a thermal source located on the leading edge of the airfoil. Pneumatic systems utilise the de-icing approach only, as they usually include an inflatable rubber ”boot” located at the leading edge of the airfoil. Whenever ice is forming on the airfoil, this ”boot” is inflated with air, causing the accreted ice to shed off the surface. An alternative to the two presented solutions is to use chemicals that are applied to the aircraft surface prior to take off. These chemicals, either dry or liquid, have the shared feature of lowering the freezing point of water. All of the systems mentioned are usually either heavy, expensive, structurally intricate, or bad for the environment, and as such, not applicable to small UAVs.

For the integration of an IPS onto a UAV specifically, several initial ideas have been published. In [5], [6], [7] an electrically and thermally conducting tape is bonded to the leading edge of an aircraft airfoil. The tape comprises a non-metallic electrical and heat-conducting layer consisting of flexible expanded graphite foil laminated to an outer thermal-conducting layer. These solutions show promising results, although power consumption is very high and no weight

considerations are presented. Another, yet similar, idea is presented in [8], where laminated resistive heaters comprising a carbon nanotube (CNT) layer, is proposed. Several compositions are presented, where one includes a liquid carrier (a paint) that facilitates the application of the composition to the substrate surface, as an aircraft wing. The solution presented in [9] introduce an IPS, where a large number of CNT arrays and patches are placed adjacent to one another on an epoxy film. This IPS nano composite layer is cured onto the precured aerosurface substrate. Wind icing tunnel tests for this specific solution show promising results.

Some carbon nano-materials (CNMs) have thermally and electrically conductive characteristics that make them exceedingly interesting as resistive heat sources [10]. Other relevant characteristics of carbon based nano-materials are superior stiffness and strength, as well as their resistance to fatigue and corrosion [11]. In [12] a fully autonomous, low power consumption, low weight, and low cost IPS is presented. The system is based on a laminated thermal source (an electrically conductive paint), where the composition includes CNMs. A copper bus bar supplies the power to the painted areas (the leading edge of the airfoil) and energy control, consequently thermal control, is achieved utilising a feedback control approach. The research presented in [12] focuses on the IP systems application on small UAVs and includes an initial, and highly simplified, thermodynamic analysis of the system that encompass the underlying airfoil structure, the surroundings (or ambient conditions), and the CNM painted area.

Research into the topic of thermodynamic analyses surrounding unheated airfoil surfaces was covered by the work presented in [13], which includes a complete temperature analysis of an unheated airfoil surface in icing conditions as a function of airspeed, altitude, ambient temperature, and liquid water content. The presented analysis is primarily significant for the design of thermal de-icing systems. Noteworthy early work into the thermodynamic analysis of airfoils and IP systems include [14]-[16].

The objective of the work presented in this paper is to conduct a thermodynamic analysis, investigating the thermal flow occurring while operating an electro thermal based IPS, integrated onto small UAVs. The study encompasses forced convection, transient conduction and thermal radiation, which are combined to produce an estimate of the heat transfer induced when activating the anti-icing solution of the IPS. The analysis includes essential parameters, such as aircraft velocity, fluid properties, free stream conditions, and various UAV platform body materials. The investigation is substantiated by numerical simulations applying a transient finite element approach to account for the multidimensional boundary conditions that vary along the chord of the airfoil. This applied approach will also account for the thermal flux into the structure of the airfoil.

The remainder of the paper is organised as follows. In Section 2 the UAV airfoils that form the structural base of the investigation are presented. A short introduction to the utilised IPS follows in Section 3. Section 4 is an explanation of the thermodynamic theory serving as the foundation for the remainder of the paper. Section 5 contain the main contribution of the paper, where numerical simulations, based on a transient finite element approach, are presented. In Section 6 the results and impacts of the numerical simulation are analysed and discussed. The paper is concluded by Section 7.

2. UAV PLATFORMS & AIRFOILS

This section provides a brief introduction to four UAV platforms displayed in Figures 1 to 4. The platforms serve as the primary test bed for the development of an IPS, as presented in [12], for small UAVs. The cruise airspeed for the four aircraft is 15 m/s to 20 m/s.

- The X8 Skywalker, developed by Skywalker Technology Co, Ltd. and integrated by the Norwegian University of Science and Technology (NTNU). The aircraft has a wingspan 2120 mm.
- The Dragoneye (DE), developed by the Naval Research Laboratory. The wingspan of the DE is 1143 mm.
- The PUMA, developed by AeroVironment. The wingspan of this platform is 2800 mm.
- The Aeromapper (AM), developed by Aeromao and operated by the The University of Alaska, Fairbanks (UAF). The wingspan of the AM is 2000 mm.

Figure 1. The X8 UAV platform.

Figure 2. The DragonEye UAV platform.

Figure 3. The PUMA UAV platform.

Figure 4. The Aeromapper UAV platform.

The structural composition of the X8 Skywalker UAV platform consists of expanded polyolefine (EPO) alone, making

it a highly durable and light weight platform. The structural composition of the DE and PUMA is identical. The core of these platforms consists of expanded polystyrene (EPS) foam covered by a thin Kevlar surface coating. Finally, the composition of the AM platform is made up of a thin skin layer of carbon fibre, covering a core of balsa. Approximate structural airfoil measurements are found in Table 1.

Table 1. Airfoil profile measurements.

Parameters [mm]	X8	DE	PUMA	AM
Surface thickness	–	0.23	0.23	0.23
Chord length (avg.)	290	305	260	210
Maximum height	41	30	26	17

Airfoils

Airfoil information on the X8, DE, and PUMA UAV platforms, required for the development of the simulation environment, is not publicly available. Consequently, airfoils that display similar characteristics, with public accessible information, have been identified. The AM airfoil is based on a standard Selig/Donovan airfoil. The airfoils identified correspond to the X8, DE, PUMA, and AM as follows.

- X8 airfoil - NACA 4412 airfoil.
- DE airfoil - Liebeck LA2573A airfoil.
- PUMA airfoil - Selig/Donovan SD7032 airfoil.
- AM airfoil - Selig/Donovan SD8020 airfoil.

The airfoil profiles are illustrated in Figures 5 to 8

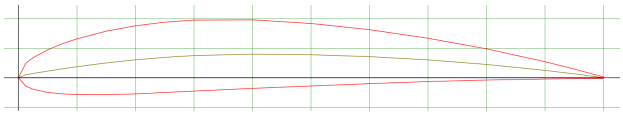

Figure 5. X8 equivalent airfoil - NACA4412

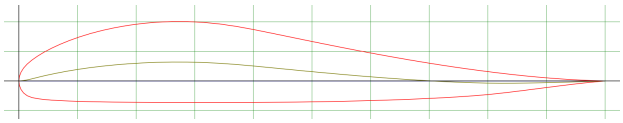

Figure 6. DE equivalent airfoil - LA2573A

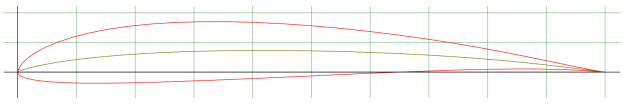

Figure 7. PUMA equivalent airfoil - SD7032

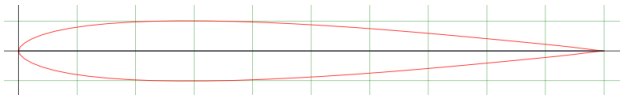

Figure 8. AM airfoil - SD8020

3. IPS-Introduction

This section summarises the IPS presented in [12], which includes the heat source investigated in this paper.

The IPS consists of an electro thermal source, a power supply and a power controller. The composition of the thermal source is based on CNMs and is applied through a liquid carrier (a paint). Resistivity of the source is based on paint thickness and painted area. Energy is supplied to the source through copper strips located on each side, along the length of the airfoil. Power is supplied to the thermal source by a standard lithium polymer battery (3-cell, 11.1V). Thermal control is achieved through power control, utilising a feedback control approach, where temperature sensors embedded in the airfoil structure supply the controller with measurements of the aerosurface temperature. The controller is primed by on-board humidity and temperature sensors, measuring environmental conditions. The IPS is completely standalone and has been developed using inexpensive, off-the-shelf products. Figures 9 and 10 illustrate how and where the IPS heat source is integrated onto the aircraft, and a diagram displaying the IPS outline.

Note that the *Profile View* in Figure 9 includes an amplification (for reasons of illustration) of how the thermal source has been applied. The thermal source thickness is in fact measured in μm. It should also be noted that in Figure 9 the *Top View* has an almost identical equivalent *Under View*.

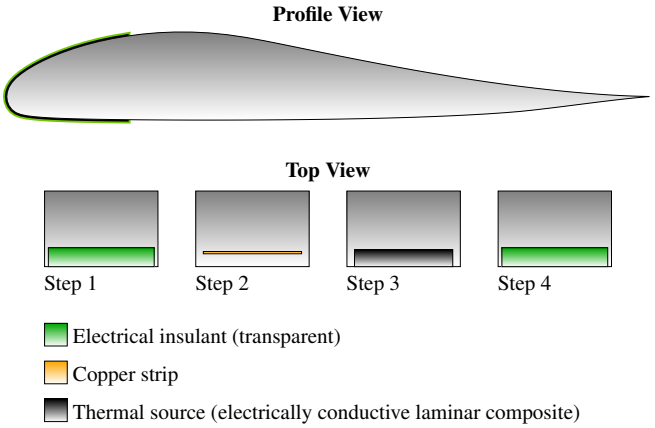

Figure 9. IPS integration. The LA2573A airfoil is used for purpose of illustration.

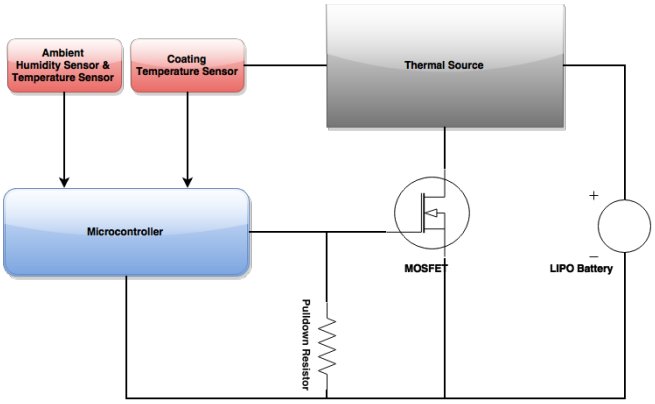

Figure 10. IPS Schematic Diagram

From a control perspective, and for the analysis presented here, the objective of the IPS is to maintain a constant temperature (above 0°C) of the thermal source.

4. THERMODYNAMIC SYSTEM

This section presents an introduction to the thermodynamic theory behind the analysis presented in this paper. The presentation cover the most important topics and details, such as diffusion for conduction, Reynolds, Nusselt and Prandtl numbers for Convection, and emissivity for radiation. For a more comprehensive presentation of thermodynamic theory the reader is referred to [17]-[22]. For a comprehensive application of the thermodynamic theory in the field of airfoil thermodynamics in icing conditions the reader is referred to the seminal work found in [13]-[16].

The investigated thermodynamic system consists of three elements, 1) the surrounding environment, i.e. a given volume of air enveloping a given airfoil, 2) the thermal source from the specific IPS, 3) a given airfoil. For two of the aircraft used in the investigation (the DE and PUMA) presented here, the latter will include two structural elements (Kevlar and EPS), as opposed to just one structural element, EPO and carbon fibre for the X8 and AM, respectively. When aircraft operations occur in non-icing conditions this specific thermodynamic system is assumed to be in thermal equilibrium, that is, there is no exchange of energy between the individual elements of the system. However, when icing occurs, consequently the thermal source is activated, energy begins to flow in the form of heat. Heat always flow from hot to cold, therefore heat begins to flow from the thermal source to the surrounding environment and into the airfoil structure. As the purpose of the IPS is to maintain the thermal source at a specific temperature, heat flowing to other parts of the thermodynamic system is considered to be dissipated. In thermodynamic theory three types of such heat flows are relevant for this investigation.

- **Thermal Conduction** - Heat flow from a solid to another solid through microscopic diffusion and collisions of particles or quasi-particles
- **Thermal Convection** - Heat flow from a solid to a fluid or gas by molecular displacement
- **Thermal Radiation** - Heat radiates from a solid to surroundings by electromagnetic waves

For a brief introduction to these concepts the reader is initially referred to the Appendix and for a thorough presentation the interested reader is referred to [17]-[22].

Note that the analysis presented here does not include any term to account for the temperature rise caused by any kinetic contributions from water impinging the aircraft surface, nor has a term been included to account for any temperature rise due to latent heat fusion. The prior has been omitted as it has been deemed an insignificant contributor [14]. The reason for the latter omission is that there should be no phase change as it is the anti-icing solution of the specified IPS that is being investigated.

5. SIMULATIONS

A transient thermodynamic analysis is conducted to predict energy performance of the selected IPS. The analysis is completed utilising the COMSOL Multiphysics commercial finite element (FE) software package. COMSOL supports fully transient, multi-dimensional, non-linear, thermal FE modelling, including temperature dependent material properties and complex boundary conditions [23].

The analysis is based on a two-dimensional model of the wing profile and will include all relevant properties regarding airfoil surface and core structure. Further, the thermal source of the IPS, applied to the leading edge of the airfoil, is modelled as a resistive heating element. The analysis encompasses three thermal transfer characteristics, 1) thermal conduction, as thermal energy is transferred from the thermal source to the surface and core structure of the airfoil, 2) thermal convection, caused by the temperature difference between ambient and the thermal source, 3) thermal radiation, due to the emissivity of the thermal source.

Assumptions

The analysis is based on the following assumptions.

A. 1: All the physical elements of the model, i.e. thermal source, airfoil surface, and airfoil core are assumed to be in perfect thermal contact

A. 2: Laminar flow near the airfoil

A. 3: Constant air pressure in the simulation environment

A. 4: Constant ambient temperature (free stream flow temperature $T_\infty = \text{constant}$)

A. 5: Uniform conditions along the span of the airfoil; This indicates that the 2D simulation environment is assumed to acquire all major aspects of the thermal response of the system. This is reasonable as the impact of differential span-directional contributions will be negligible compared to chord-directional contributions.

Numerical Analysis

Using the COMSOL Multiphysics software package, a simulation environment was developed, corresponding to that of the controlled environment in a wind icing tunnel. The virtual wind icing tunnel (VWIT) developed measures 1m in width and 0.5m in height. Inlet airspeed (u_∞) is between 10 m/s and 20 m/s, ambient VWIT temperature (T_∞) ranges from -5°C to -20°C, and liquid water content is 1.1g/m^3 [9]. The set temperature for the thermal source (T_s) of each airfoil is 5°C. For the purpose of simulation validity the thermal source is activated using a smoothing function (increasing from 0 to 1) enabling full power usage after $t = 15$ seconds. The simulation time is $t = 60$ seconds. Table 2 shows the maximum total power dissipated (q_d [W]), as a consequence of thermal conduction, convection, and radiation, for each UAV platform, with varying T_∞ and u_∞.

Table 2. Maximum power dissipation for each UAV platform, with varying T_∞ and u_∞

VWIT		X8	DE	PUMA	AM
T_∞ [°C]	u_∞ [m/s]	(q_d [W])			
-20.0	20.0	120.96	89.21	90.51	65.41
-15.0	20.0	101.87	73.36	72.89	53.49
-10.0	20.0	83.22	57.79	56.47	41.83
-5.0	20.0	66.00	42.80	40.48	30.38
-20.0	17.5	105.69	80.52	80.69	56.98
-20.0	15.0	90.70	71.46	71.77	48.73
-20.0	12.5	75.20	62.61	62.79	40.34
-20.0	10.0	60.01	45.08	44.84	32.05

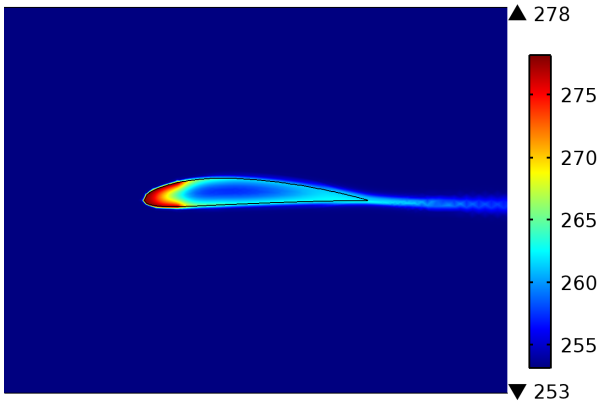

Figure 11. Thermal dissipation of the X8 platform, with fixed thermal source temperature, $T_s = 5°\text{C}$, $T_\infty = -20°\text{C}$, and $u_\infty = 20$ m/s

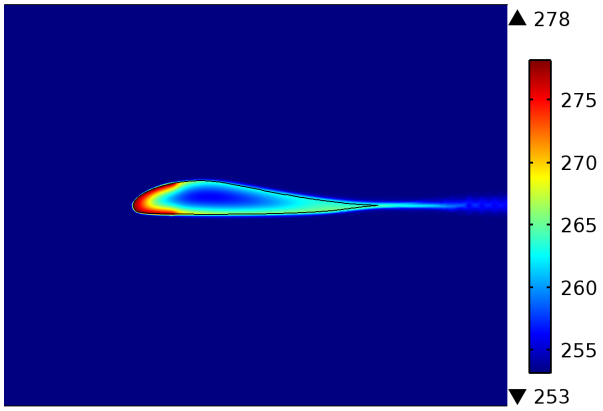

Figure 12. Thermal dissipation of the DE platform, with fixed thermal source temperature, $T_s = 5°\text{C}$, $T_\infty = -20°\text{C}$, and $u_\infty = 20$ m/s

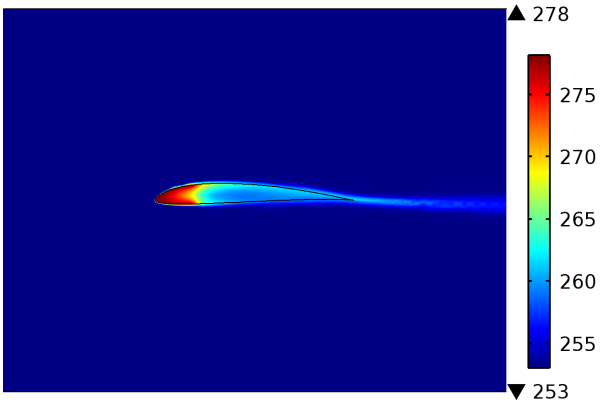

Figure 13. Thermal dissipation of the PUMA platform, with fixed thermal source temperature, $T_s = 5°\text{C}$, $T_\infty = -20°\text{C}$, and $u_\infty = 20$ m/s

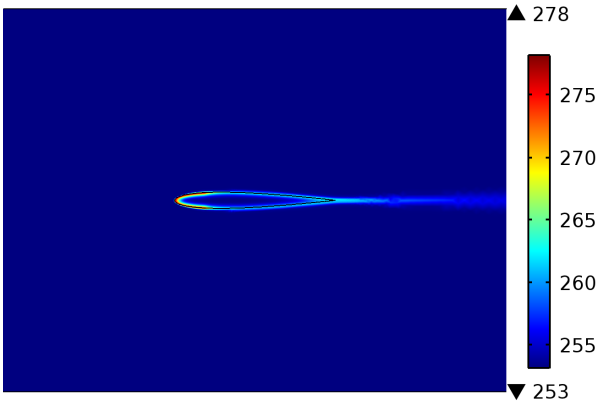

Figure 14. Thermal dissipation of the AM platform, with fixed thermal source temperature, $T_s = 5°\text{C}$, $T_\infty = -20°\text{C}$, and $u_\infty = 20$ m/s

Figures 11 to 14 display the thermal dissipation along and into the four platform airfoils, where the thermal source temperature is controlled to be fixed at $T_s = 5°\text{C}$. The colour legend to the right in each figure is in temperature unit Kelvin.

For the purpose of perspective simulations have been conducted, where the thermal source, rather than having a specified temperature, have a specified power supplied. The power supplied to the thermal source (P_s [W/m^2]) of each airfoil is 10 kW/m^2, approximately corresponding to [9]. Again for the purpose of simulation validity the thermal source is activated using the aforementioned smoothing function enabling full power usage after $t = 15$ seconds, with total simulation time $t = 60$ seconds. The resulting thermal images are displayed in Figures 15 to 18.

6. Discussion

As illustrated by Figures 11 to 14 and quantified in Table 2 a high airspeed and a low ambient temperature results in a larger power level required to achieve the desired temperature of the thermal source, with $T_\infty = -20°\text{C}$ and $u_\infty = 20$ m/s resulting in the largest dissipation for all the platform airfoils. It is worth noting that the impact of ambient temperature variations is less than the impact of varying airspeeds, as a 50% decrease in ambient temperature results in an approximate 31%, 35%, 38%, and 36% decrease in thermal dissipation for the X8, DE, PUMA, and AM, respectively, whereas a 50% decrease in airspeed results in an approximate 50% decrease, for all the platforms, in thermal dissipation.

The considerable difference in thermal dissipation, seen when comparing the X8 platform to the remaining three, is primarily a consequence of the structural design of the X8 airfoil that leads to a thicker boundary layer, increasing the thermal conduction into this layer.

The simulations resulting in Figures 15 to 18 display the thermal dissipation for the four platform UAVs when a given power is specified, as opposed to a specific temperature. The simulation were conducted to identify any uniformity

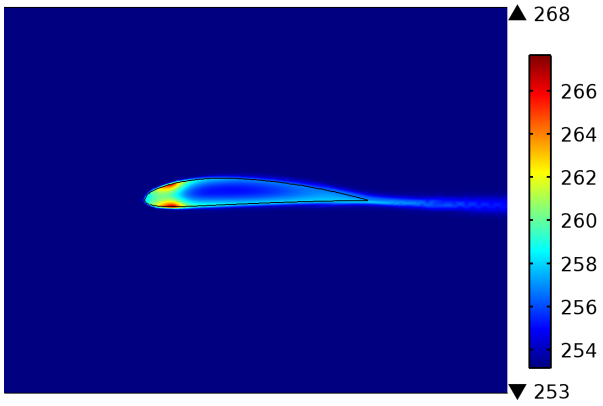

Figure 15. Thermal dissipation of the X8 platform, with fixed power supply, $P_s = 10$ kW/m^2, $T_\infty = -20$ °C, and $u_\infty = 20$ m/s

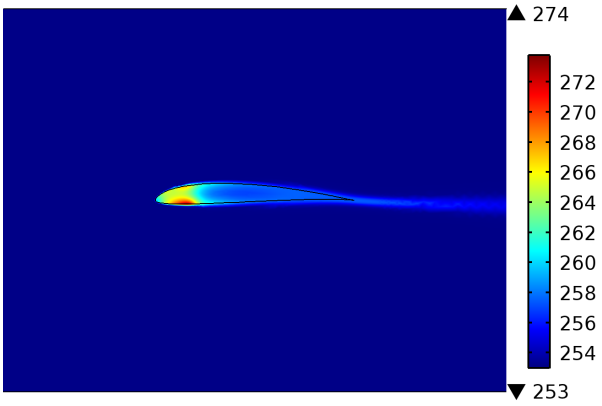

Figure 17. Thermal dissipation of the PUMA platform, with fixed power supply, $P_s = 10$ kW/m^2, $T_\infty = -20$ °C, and $u_\infty = 20$ m/s

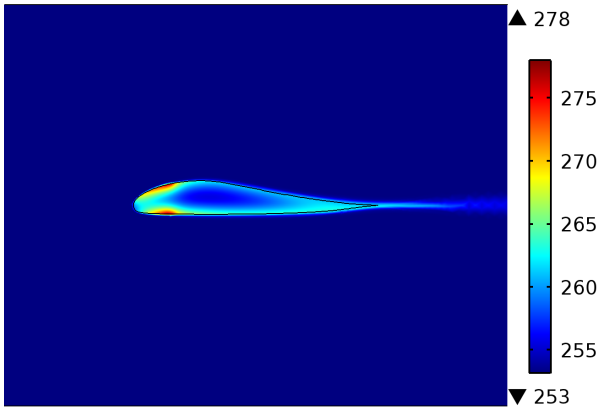

Figure 16. Thermal dissipation of the DE platform, with fixed power supply, $P_s = 10$ kW/m^2, $T_\infty = -20$ °C, and $u_\infty = 20$ m/s

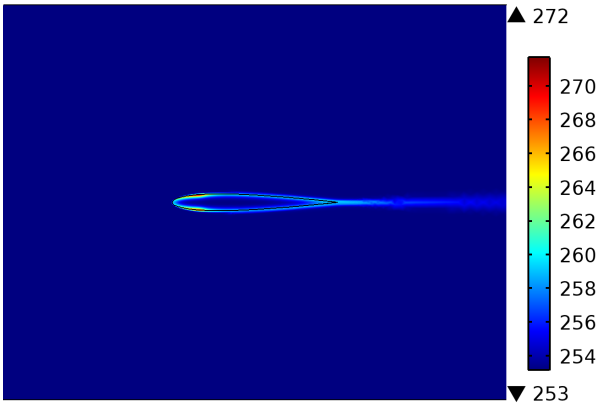

Figure 18. Thermal dissipation of the AM platform, with fixed power supply, $P_s = 10$ kW/m^2, $T_\infty = -20$ °C, and $u_\infty = 20$ m/s

issues. As seen the thermal dissipation is not uniform over the thermal source located on the leading edge of the airfoil, i.e. a higher level of power is required to maintain a given temperature at the absolute leading edge of an airfoil, as opposed to the power required further back along the chord length of that airfoil. This property suggests the need for a more diverse layout of the thermal source, where another method of intelligent control could be beneficial to minimise power consumption.

7. Conclusion

Optimising power consumption for any IPS relying on a resistive thermal source is imperative for small UAVs operating in regions, where potential icing conditions are frequent.

The work presented here constitutes a first step in reaching that objective, as a thermodynamic analysis is conducted of a specified anti-icing IPS based on an electrically conductive composite, laminated onto the leading edge of airfoils. Using the COMSOL Multiphysics software package a virtual wind icing tunnel was developed as a controlled test simulation environment. The primary focus has been on identifying a maximum power dissipation, for a fixed thermal source temperature ($T_\infty = 5$°C), manifested in thermal conduction, thermal convection and radiation, for four different UAV platforms, imposing varying flight conditions, i.e. various ambient temperature and airspeed.

As expected, all four UAV platforms displayed maximum power dissipation at the minimum ambient temperature ($T_\infty = -20$°C) and maximum airspeed ($u_\infty = 20$ m/s), with the X8 having the largest dissipation. The reason for the characteristics of this particular platforms is attributed to a thicker boundary layer, resulting in a maximum power dissipation of 120.96 W.

Another type of simulations were conducted, where the objective was to investigate the uniformity of the temperature along the thermal source, when applying a fixed power source ($P_s = 10$kW/m^2). These simulations revealed that the temper-

ature is not uniform along the thermal source, which opens up for the possibility of a more diverse layout of the thermal source, where another method of intelligent control could be beneficial to minimise power consumption.

APPENDIX

Thermal Conduction

Thermal conduction is the transfer of internal energy by microscopic diffusion and collision of particles or quasi-particles, thereby transferring kinetic and potential energy (collectively denoted internal energy). Thermal conduction occurs within a single object or material, or between multiple objects in contact with each other.

Joseph Fourier was the first to formulate a complete exposition on the theory of heat conduction, where he stated the empirical law, now known as Fourier's law: *the heat flux, q* [W/m^2]*, resulting from thermal conduction is proportional to the magnitude of the temperature gradient and opposite to it in sign* [17]. Utilising k [W/(m·K)] as the constant of proportionality, denoted the thermal conductivity , Fourier's law can be written as

$$\vec{q} = -k \cdot \nabla T, \tag{1}$$

where T is the temperature in Kelvin. In general the coefficient of proportionality k - the thermal conductivity - also depends on position and temperature, i.e. $k = k(\vec{r}, T(\vec{r},t))$, where $\vec{r}$ is the position vector. The temperature gradient ∇T describes both magnitude and direction of the maximum temperature change at each point and is defined as

$$\nabla T \equiv \vec{i}\frac{\partial T}{\partial x} + \vec{j}\frac{\partial T}{\partial y} + \vec{k}\frac{\partial T}{\partial z}. \tag{2}$$

Utilising Fourier's law, the first law of thermodynamics (the law of energy conservation), and Gauss' theorem the following expression is obtained[2],

$$\nabla \cdot k\nabla T + \dot{q} = \rho c\frac{\partial T}{\partial t}, \tag{3}$$

Where ρ is the density of a given medium (gas, fluid, or solid) and c is the specific heat capacity of the same medium. Equation (3) is known as the *heat diffusion equation* in three dimensional space, which is valid under the constraint of two assumptions:

- Incompressible medium
- No convection (The medium cannot undergo any relative motion)

If the variation of k with T is small, Equation (3) can be rewritten into

$$\nabla^2 T + \frac{\dot{q}}{k} = \frac{1}{\alpha}\frac{\partial T}{\partial t}, \tag{4}$$

where α [m^2/s] is the thermal diffusivity, which is given by

$$\alpha = \frac{k}{\rho c}. \tag{5}$$

The thermal diffusivity is a measure of the rate at which a medium distributes heat away from a thermal source. As materials in general are not heated instantaneously α includes both the thermal conductivity k and the volumetric heat capacity ρc.

From Equation (4), the expression $\nabla^2 T = \nabla \cdot \nabla T$ is known as the Laplacian and in a Cartesian coordinate system is given by

$$\nabla^2 T = \frac{\partial^2 T}{\partial x^2} + \frac{\partial^2 T}{\partial y^2} + \frac{\partial^2 T}{\partial z^2} \tag{6}$$

Equation (4) is recognised as a complete multidimensional transient heat conduction equation [17].

Thermal Convection

Thermal convection occurs as energy transfer due to diffusion and by bulk (or macroscopic) motion of a fluid or gas. This motion is attributed to large number of molecules moving collectively or as aggregates. In the presence of a temperature gradient such motion contributes to the transfer of thermal energy. As molecules in aggregate maintain their random motion, the combined thermal transfer is due to the superposition of energy transferral by random motion of the molecules and the bulk motion of the fluid or gas [18].

An alternative description of the physical process of thermal convection from [17], [19] follows. Consider a cool gas (or fluid) flowing past a warm body. The gas immediately adjacent to the body forms a layer of thickness δ, which flow at a reduced velocity. This layer is know as the *boundary layer*. Heat is conducted into the boundary layer, which transports it farther downstream, where it is mixed with the cooler free stream flowing gas. This process, where heat is transported by a moving gas is called convection. The mathematical representation of convection attributed to Sir Isaac Newton is given by

$$q = \bar{h}\Delta T, \tag{7}$$

where $\Delta T \equiv (T_s - T_\infty)$. Equation (7) is the steady-state form of what is known as Newton's law of cooling [20], [21], where T_s is the solid' surface temperature and T_∞ is the temperature of the oncoming flow of gas. The coefficient $\bar{h}$ [W/(mK)] is termed the *convective heat transfer coefficient*, where the bar signifies that it is the average of coefficients over the surface of a body. Without the bar, h is simply a local value at a specific point on the body surface. The convective heat transfer coefficient is a highly intricate quantity to predict and it is tightly linked to the motion of the gas around the body that is heated or cooled.

The boundary layer can be in either a turbulent or laminar flow regime, where the latter is characterised by the gas flowing in parallel layers, i.e. there is no transferral of gas particles between the parallel layers, nor any swirls or eddies [24]. Properties concerning the laminar flow regime is a high momentum of diffusion and a lower momentum of convection [17], [19], [25]. The work presented in this paper is based on the assumption that the flow around relevant areas of a given airfoil is laminar.

It is evident that thermal convection is highly interconnected with fluid dynamics, therefore significant parameters necessitate an introduction. One such parameter is a dimensionless quantity that aides the characterisation and quantification of different flow regimes and is known as the Reynolds number, Re, which is defined as the ratio of momentum forces to viscous forces. Laminar flow generally occurs at low Reynolds numbers (though still at Re$> 10^4$ for airfoils [26]), where

[2]The interested reader is referred to [17] for the complete derivation.

viscous forces are more dominant, or where the flow velocity is less dominant. For flow around airfoils Re is defined as

$$\mathrm{Re} = \frac{u_\infty x_c}{\nu}, \tag{8}$$

where u_∞ is the free stream flow velocity, x_c is a characteristic linear dimension (for airfoils this corresponds to the chord line) , and ν is the kinematic viscosity of the gas or fluid in which the airfoil operates.

When a temperature difference exists between a solid and the free stream of a fluid or gas flowing past, a thermal boundary layer is present, with thickness δ_t, different from the thickness of the boundary layer δ. Heat transferral at the surface is by conduction and, as such

$$-k_f \left.\frac{\partial (T - T_s)}{\partial y}\right|_{y=0} = h\,(T_s - T_\infty)\,, \tag{9}$$

where k_f is the conductivity of the fluid or gas, T is the temperature at a given point in the the thermal boundary layer, and y is a perpendicular distance from the surface of the solid. The term on the left of the equality correspond to Fourier's law (of thermal conduction) in one-dimensional space. Rearranging Equation (9) and multiplying by the inverse of a characteristic linear dimension results in

$$\frac{hx_c}{k} = \frac{\left.\frac{\partial (T_s - T)}{\partial y}\right|_{y=0}}{\frac{(T_s - T_\infty)}{x_c}} \equiv \mathrm{Nu}_{x_c}, \tag{10}$$

which is known as the *Nusselt number* and can be summarised as the ratio of conductive thermal resistance to the convective thermal resistance of the fluid [19]. The temperature profile for a fluid or gas flowing past a heated solid surface is illustrated in Figure 19.

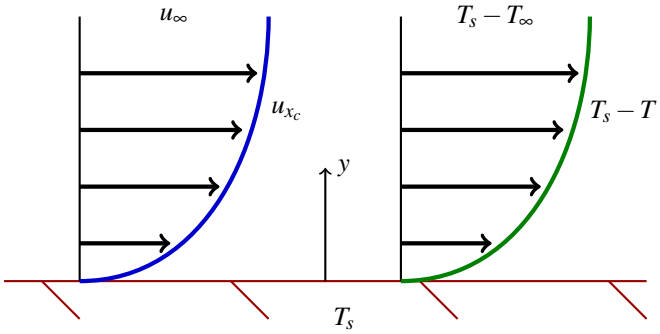

Figure 19. Temperature and velocity profiles for a fluid or gas flowing past a heated plate.

A Nusselt number close to 1 signifies laminar flow, where larger values for Nu corresponds to a turbulent flow.

The final significant parameter introduced here is the *Prandtl number* Pr, which can be summarised as the ratio of molecular kinematic viscosity to the molecular thermal diffusivity [19], and is defined as

$$\mathrm{Pr} \equiv \frac{\nu}{\alpha}. \tag{11}$$

The values of the Prandtl number indicate the interrelation between the thickness of the boundary layer and the thickness of the thermal boundary layer. If $\mathrm{Pr} = 1$ it indicates $\delta = \delta_t$, further when $\mathrm{Pr} > 1$, $\delta > \delta_t$, and conversely when $\mathrm{Pr} < 1$, $\delta < \delta_t$. Intuitively this is sensible as high viscosity leads to a thick boundary layer, and a high thermal diffusivity should imply a thick thermal boundary layer.

Thermal convection is generally divided into two main classifications. These are related to the driving force causing the flow. For the work presented in this paper focus will be limited to *forced convection*, as opposed to *free* or *natural convection*. Forced convection is the classification applied for describing convection, where fluid or gas circulation is produced by an external agent, such as wind, a fan, or the forced movement of a body through a fluid or gas.

Thermal Radiation

Thermal radiation is electromagnetic radiation generated by particle collision that cause the kinetic energy of atoms and molecules to change. It is this change that results in a charge-acceleration and/or dipole oscillation, which in turn produce the electromagnetic radiation [**?**].

Thermal radiation differs from conduction and convection in several ways, but most prominently in that no medium is required for its propagation. In fact maximum thermal radiation is achieved when the transferral of energy is in perfect vacuum. The perfect thermal radiator is termed a *black body* and has the properties that it absorbs all incident energy that reaches it and reflects nothing [19]. Black bodies do, however, emit energy as electromagnetic waves at wavelengths $0.1 - 100\mu m$. The energy emission, $e(T)$ [W/m^2], from a black body is given by

$$e_b(T) = \sigma T^4, \tag{12}$$

where T is the absolute temperature and the proportionality constant σ is the Stefan Boltzmann constant, which equals 5.676×10^{-8} $[\mathrm{W}/(\mathrm{m}^2 \cdot K)]$. Equation (12) is most often referred to as the *Stefan Boltzmann law* of thermal radiation. For a body that do not display the same energy characteristics as a black body, the expression found in Equation (12) will not suffice, another parameter is required. The total energy emission, $e(T)$, of a given body surface is defined as the total rate of thermal energy emitted by radiation from that surface in all directions and at all wavelengths per unit surface area [19]. Closely related to the total energy emission is the emissivity ε, which is defined as

$$\varepsilon \equiv \frac{e(T)}{e_b(T)}, \quad 0 < \varepsilon \leq 1, \tag{13}$$

consequently the total energy emitted per unit surface area can be written as

$$e(T) = \varepsilon e_b(T) = \varepsilon \sigma T^4. \tag{14}$$

It is evident that $\varepsilon = 1$ for a black body. For the electrically conductive laminar composite utilised as thermal source in the work presented here the emissivity is approximately $\varepsilon = 0.90$ [19].

ACKNOWLEDGEMENTS

This work has been carried out at the Centre for Autonomous Marine Operations and Systems (AMOS), supported by the

Research Council of Norway through the Centres of Excellence funding scheme, Project number 223254 - AMOS. The Norwegian Research Council is acknowledged as the main sponsor of AMOS.

Deep gratitude needs to be expressed to Matthew Fladeland, programs manager at the airborne science program, at NASA-Ames research center, for sharing his expertise, assistance, and support during the completion of the research presented here. The same should go to Eyal Saiet, remote sensing specialist, at the University of Alaska, Fairbanks, for sharing his assistance and support. Appreciation should also go to Anne Nuijten, researcher at the department of Civil and Transport Engineering, Norwegian University of Science and Technology, for sharing her experiences, ideas, and support. Finally, gratitude needs to be expressed to Erlend Kristiansen from COMSOL Multiphysics, for his patience and assistance in the development of the simulation environment.

REFERENCES

[1] F. S. Leira, T. A. Johansen, and T. I. Fossen, "Automatic detection, classification and tracking of objects in the ocean surface from uavs using a thermal camera," in *Aerospace Conference, 2015 IEEE*, 2015, pp. 1–10.

[2] S. G. Cober, G. A. Isaac, and J. W. Strapp, "Characterizations of aircraft icing environments that include supercooled large drops," *Journal of Applied Meteorology*, vol. 40, no. 11, pp. 1984–2002, 2001.

[3] M. K. Politovich, "Aircraft icing caused by large supercooled droplets," *Journal of Applied Meteorology*, vol. 28, no. 9, pp. 856–868, 1989.

[4] R. Siquig, "Impact of icing on unmanned aerial vehicle (uav) operations," DTIC Document, Tech. Rep., 1990.

[5] O. Hastings and O. Hastings, "Electrically conductive laminate for temperature control of aircraft surface," sep 1994, U.S Patent 5,344,696. [Online]. Available: https://www.google.no/patents/US5344696

[6] R. Rutherford and R. Dudman, "Zoned aircraft deicing system and method," may 2001, U.S. Patent 6,237,874. [Online]. Available: https://www.google.no/patents/US6237874

[7] R. Rutherford, "De-ice and anti-ice system and method for aircraft surfaces," feb 2001, U.S. Patent 6,194,685. [Online]. Available: https://www.google.no/patents/US6194685

[8] A. Heintz, A. Christiaen, B. Vijayendran, J. Elhard, R. Lalgudi, W. Robbins, A. Gupta, and J. Cafmeyer, "Electrically conductive coating composition," nov 2013, U.S. Patent 8,581,158.

[9] S. T. Buschhorn, S. S. Kessler, N. Lachmann, J. Gavin, G. Thomas, and B. L. Wardle, *Electrothermal Icing protection of Aerosurfaces Using Conductive Polymer Nanocomposites*. American Institute of Aeronautics and Astronautics, 2013.

[10] Z. Han and A. Fina, "Thermal conductivity of carbon nanotubes and their polymer nanocomposites: A review," *Progress in Polymer Science*, vol. 36, no. 7, pp. 914 – 944, 2011.

[11] S. S. Wicks, R. G. de Villoria, B. L. Wardle, S. S. Kessler, and C. T. Dunn, "Carbon nanotube (cnt) enhancements for aerosurface state awareness," in *Proceedings of the Workshop on Structural Health Monitoring, 2011 8th annual IWSHM*, September 2011.

[12] K. L. Sørensen, A. S. Helland, and T. A. Johansen, "Carbon nanomaterial-based wing temperature control system for in-flight anti-icing and de-icing of unmanned aerial vehicles," in *IEEE Aerospace Conference*, March 2015, pp. 1–6.

[13] B. L. Messinger, "Equilibrium temperature of an unheated icing surface as a function of air speed," *Journal of the Aeronautical Sciences*, vol. 20, no. 1, pp. 29–42, 1953.

[14] N. R. Bergrun, D. Jukoff, B. A. Schlaff, and J. Neel, Carr B., "The calculation of the heat required for wing thermal ice prevention in specified icing conditions," National Advisory Committee for Aeronautics. Ames Aeronautical Lab.; Moffett Field, CA, United States, Tech. Rep., December 1947.

[15] J. K. Hardy, "An analysis of the dissipation of heat in conditions of icing from a section of the wing of the c-46 airplane," National Advisory Committee for Aeronautics. Ames Aeronautical Lab.; Moffett Field, CA, United States, Tech. Rep., January 1945.

[16] T. F. Gelder and J. P. Lewis, "Comparison of heat transfer from airfoil in natural and simulated icing conditions," National Advisory Committee for Aeronautics, Lewis Flight Propulsion Laboratory, United States, Tech. Rep., September 1951.

[17] J. H. L. IV and J. H. L. V, *A Heat Transfer Textbook*. Phlogiston Press, 2015.

[18] F. Incropera, *Introduction to heat transfer*. John Wiley & Sons, Inc, 2007.

[19] J. R. Welty, C. E. Wicks, R. E. Wilson, and G. L. Rorrer, *Fundamentals of Momentum, Heat, and Mass Transfer*, 5th ed. John Wiley & Sons, Inc, 2007.

[20] C. P. Kothandaraman, *Fundamentals of Heat and Mass Transfer*, 3rd ed. New Age International Limited, Publishers, 2006.

[21] D. Kondepudi, *Introduction to Modern Thermodynamics*, 1st ed. John Wiley & Sons, Inc, 2008.

[22] R. Siegel, *Thermal radiation heat transfer*. Taylor & Francis, 2002.

[23] C. 5.1, *Heat Transfer Module User's Guide*, 2015. [Online]. Available: http://www.ewp.rpi.edu/hartford/~collir5/MP/OTHER/Reference/HeatTransferModuleUsersGuide.pdf

[24] C. Geankoplis, *Transport Processes and Separation Process Principles (Includes Unit Operations) Fourth Edition*, 4th ed. Prentice Hall Press, 2003.

[25] D. Rogers, *Laminar flow analysis*. Cambridge University Press, 1992.

[26] Y. Lian and W. Shyy, "Laminar-turbulent transition of a low reynolds number rigid or flexible airfoil," *AIAA Journal*, vol. 45, no. 7, pp. 1501–1513, 2007.

[27] K. Al-Khalil, L. Salamon, and G. Tenison, *Development of the Cox Icing Research Facility*. American Institute of Aeronautics and Astronautics, 1998.

[28] F. Morency, F. Tezok, and I. Paraschivoiu, "Heat and mass transfer in the case of anti-icing system simulation," *Journal of Aircraft*, vol. 37, no. 2, pp. 245–252, 2000.

BIOGRAPHY

Kim Lynge Sørensen *received his B.Sc. and M.Sc. degrees in electrical engineering, specialising in robot technology, from the Technical University of Denmark in 2011 and 2013, respectively. In 2013 he began his PhD when he became a member of the centre for Autonomous Marine Operations and Systems, Department of Engineering Cybernetics, at the Norwegian University of Science and Technology, where his current research primarily revolves around icing on UAVs.*

Tor Arne Johansen *received his M.Sc. degree in 1989 and Ph.D. degree in 1994, both in electrical and computer engineering from the Norwegian University of Science and Technology. He worked at SINTEF Electronics and Cybernetics as a researcher before he was appointed Associated Professor in Engineering Cybernetics at the Norwegian University of Science and Technology in 1997 and was promoted to Professor in 2001. In December 2002 Prof. Johansen co-founded the company Marine Cybernetics AS, where he was Vice President until 2008. Prof. Johansen received the 2006 Arch T. Colwell Merit Award of the SAE. He is currently a key member of the scientific staff at the centre for Autonomous Marine Operations and Systems, at the Norwegian University of Science and Technology.*